Applied Catalysis B: Environmental 164 (2015) 128–134

Contents lists available at ScienceDirect

Applied Catalysis B: Environmental

journal homepage: www.elsevier.com/locate/apcatb

Influence of Ir content on the activity of Pt-Ir/C catalysts for hydrogen iodide decomposition in iodine–sulfur cycle

Laijun Wang[a,*], Qi Han[b], Songzhi Hu[a], Daocai Li[a], Ping Zhang[a], Songzhe Chen[a], Jingming Xu[a], Baijun Liu[b]

[a] Institute of Nuclear and New Energy Technology, Tsinghua University, Beijing 102201, PR China
[b] College of Chemical Engineering, China University of Petroleum, Beijing 102249, PR China

ARTICLE INFO

Article history:
Received 8 July 2014
Received in revised form 27 August 2014
Accepted 5 September 2014
Available online 16 September 2014

Keywords:
Hydrogen iodide decomposition
Thermochemical hydrogen production
Iodine–sulfur cycle
Supported Pt-Ir catalysts
Characterization

ABSTRACT

This study aimed to determine the influence of Ir content on the behavior of Pt-Ir/C catalysts for hydrogen iodide decomposition in iodine–sulfur thermochemical water-splitting cycle. A series of bimetallic *x*Pt-*y*Ir/C catalysts (x = 4, 3, 2.5, 2, 1 wt.%; y = 1, 2, 2.5, 3, 4 wt.%) were prepared by co-impregnation and reduction method. For comparison, monometallic 5%Pt/C and 5%Ir/C catalysts were also prepared. The catalysts were characterized by X-ray diffraction and transmission electron microscopy. Changing the Ir content in the bimetallic Pt-Ir/C catalysts can modify the particle size and dispersion state of the supported metal nanoparticles. The results of the characterizations of the fresh and used catalysts indicated that the size of the Pt nanoparticles has significantly increased after HI decomposition whereas that of the Pt-Ir nanoparticles is more resistant to particle growth. Among the Pt, Ir, and binary Pt-Ir catalysts, the bimetallic 2.5%Pt-2.5%Ir/C exhibited the highest catalytic activity toward HI decomposition. The 70 h durability test showed that the Pt-Ir bimetallic catalyst possessed good activity maintenance.

1. Introduction

The catalytic decomposition of hydrogen iodide is an important reaction for producing hydrogen in iodine–sulfur thermochemical water-splitting (IS) cycle [1], which is composed of the Bunsen reaction (1), sulfuric acid decomposition (2), and HI decomposition (3).

Bunsenreaction(exothermic, 80–120 °C) :

$$SO_2 + I_2 + 2H_2O \leftrightarrow 2HI + H_2SO_4 \quad (1)$$

H_2SO_4decomposition(endothermic, 800–900 °C) :

$$H_2SO_4 \leftrightarrow SO_2 + 1/2O_2 + H_2O \quad (2)$$

* Corresponding author. Tel.: +86 10 80194036; fax: +86 10 62771740.
E-mail addresses: wanglaijun@mail.tsinghua.edu.cn (L. Wang), hq_8933@163.com (Q. Han), husz13@mails.tsinghua.edu.cn (S. Hu), 07ldc@163.com (D. Li), zhangping77@mail.tsinghua.edu.cn (P. Zhang), chenszh@mail.tsinghua.edu.cn (S. Chen), xujingming@mail.tsinghua.edu.cn (J. Xu), bjliu@cup.edu.cn (B. Liu).

http://dx.doi.org/10.1016/j.apcatb.2014.09.018
0926-3373/

$$\text{HIdecomposition(endothermic, 400–500 °C)} : 2HI \leftrightarrow H_2 + I_2 \quad (3)$$

The IS cycle was originally developed by General Atomics in 1970s. Given that this cycle has several advantages, such as high efficiency, zero emission, full liquid/gas phase operation, and suitable maximum temperature (good matching with high-temperature gas-cooled reactor), the IS cycle is one of the most promising alternative methods for large-scale hydrogen production; the IS cycle has been extensively investigated over the past few decades by different institutes in Japan, USA, France, Korea, Italy, India, and China [1–5].

Although much progress has been made on the chemistry, materials, flow sheet simulations, and process engineering of the IS cycle, some scientific and technical problems remain unsolved [6], including the HI catalytic decomposition. Among the three reactions of the IS cycle, the HI decomposition possesses a relatively low equilibrium conversion (its equilibrium conversion at 500 °C is ~23%) and a low reaction rate, even at high reaction temperatures. The use of suitable catalysts can promote HI decomposition to achieve workable reaction rates. Different catalytic materials have been investigated for this reaction [7]. Active carbon (AC), supported Ni, and supported Pt group metals have been used to catalyze HI decomposition [3,7–12]. In particular, AC-supported Pt catalysts exhibit excellent catalytic performance and have been used in the IS demonstrations at the Japan Atomic Energy Agency and the Institute of Nuclear and New Energy Technology, Tsinghua University [7,13,14]. However, supported Pt monometallic catalysts are expensive and limited in supply. The stability of the supported Pt monometallic catalysts is also undesirable because the monometallic Pt nanoparticles tend to sinter during HI decomposition at high temperatures, which may decrease the catalytic performance [9,12]. Therefore, the stability and performance of the supported Pt monometallic catalysts should be improved for HI decomposition.

Compared with the monometallic Pt catalysts, bimetallic Pt-based catalysts, which are relatively cheap, often show distinct electronic and chemical properties, better catalytic performances, and higher stability. Therefore, the Pt-based bimetallic catalysts have been widely used as alternative to monometallic Pt catalysts in various catalytic and electrocatalytic reactions [15,16]. Up to date, several Pt-based bimetallic catalysts have been investigated, such as Pt-Ir, Pt-Ni, Pt-Sn, and Pt-Pd, and most of these catalysts possess improved properties relative to monometallic Pt catalysts [15–17]. In the case of Pt-Ir catalysts, Ir is more readily reduced than Pt and is always present as an Ir metal [17]. Metallic Ir is also more active for hydrogenolysis and more sensitive to pre-sulfiding than Pt [18]. Thus, bimetallic Pt-Ir catalysts are commonly used in various catalytic reactions, such as reduction, hydrogenation, hydrogenolysis, and reforming. Yang et al. [19] proved that the formed Pt-Ir bimetallic clusters inside the NaY zeolite supercage exhibit specific characteristics that are different from those of Pt and Ir monometallic clusters. They also found that Pt-Ir/NaY bimetallic catalysts exhibit improved activity maintenance compared with that of Pt/NaY monometallic catalyst in *n*-heptane reforming reaction [20]. Macleod et al. [17] reported that metallic Ir is sintered much less readily in hydrogen at 510 °C than metallic Pt. They also proved that Pt-Ir is highly resistant to deactivation, because metallic Ir provides sites for hydrogenation/hydrogenolysis of coke fragments. D'Ippolito et al. [21] reported that Pt-Ir bimetallic catalysts exhibit an adequate metal/acid balance and are more suitable for naphthenic ring opening than Pt monometallic catalysts.

In our previous work [22], we investigated the performance of Pt-Ir/C catalysts prepared by electroless plating method for HI decomposition. These catalysts show much higher catalytic activity and thermostability during HI decomposition. To determine the role of Ir and its composition on catalyst performance, we conduct a comparative study of various bimetallic *x*Pt-*y*Ir/C catalysts ($x = 4, 3, 2.5, 2, 1$ wt.%; $y = 1, 2, 2.5, 3, 4$ wt.%). The present study mainly aims to investigate the function of Ir in the bimetallic Pt-Ir/C catalysts and to obtain suitable catalysts for long-term performance test in HI decomposition by optimizing the composition of the bimetallic Pt-Ir/C catalysts.

2. Experimental

2.1. Catalyst preparation

The applied AC support (1471.1 m^2/g, 40–60 mesh, Xilong Chemical Company) was directly dried in air at 120 °C for 4 h. Hexahydrate chloroplatinic acid ($H_2PtCl_6 \cdot 6H_2O$, analytical reagent, Shanghai Guanghua Technology Co., Ltd.) and chloroiridic acid ($H_2IrCl_6 \cdot 6H_2O$, analytical reagent, Beijing General Research Institute of Nonferrous Metals) were used as precursors for Pt and Ir, respectively. The AC-supported Pt-Ir bimetallic catalysts were prepared by co-impregnation and reduction method. Appropriate amounts of AC were impregnated with specified amount of an aqueous solution containing hexachloroplatinic acid and chloroiridic acid to obtain the desired metal loading of 5.0 wt.%. After impregnation, the samples were oven dried at 120 °C for 4 h. The resulting solid was reduced by KBH_4 aqueous solution at room temperature for 30 min, filtrated and washed thoroughly with distilled water, and then dried in air at 120 °C for 4 h. Based on the metal weight loadings, the catalysts were labeled as 4%Pt-1%Ir/C, 3%Pt-2%Ir/C, 2.5%Pt-2.5%Ir/C, 2%Pt-3%Ir/C, and 1%Pt-

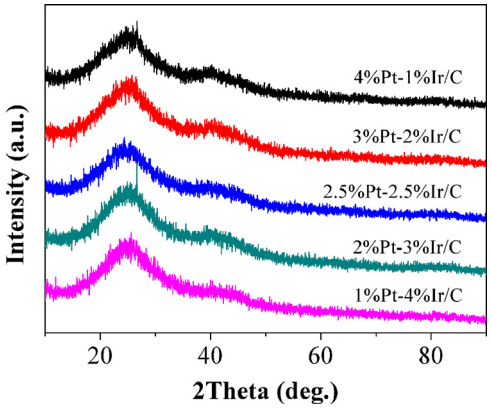

Fig. 2. The XRD patterns of the active carbon supported bimetallic Pt-Ir catalysts.

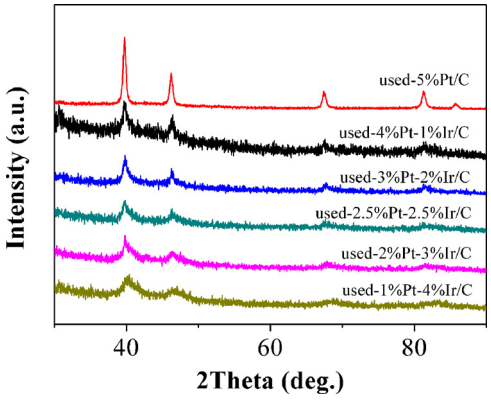

Fig. 3. XRD patterns of the used-5%Pt/C and the used Pt-Ir/C bimetallic catalysts.

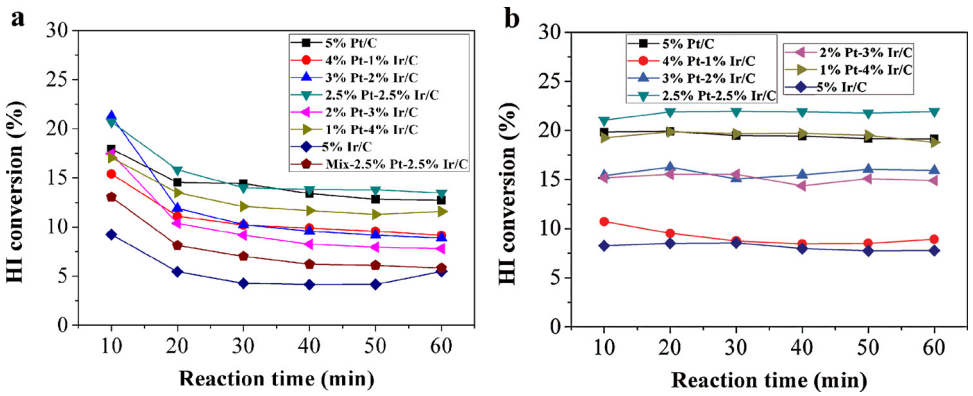

Fig. 1. HI conversions over different catalysts at (a) 400 °C and (b) 500 °C with the reaction time.

4%Ir/C. For comparison, monometallic 5%Pt/C and 5%Ir/C catalysts were also prepared by impregnation–reduction method.

2.2. Catalyst characterization

Powder X-ray diffraction (XRD) and Brunauer–Emmett–Teller (BET) surface area measurements were performed as described previously [9,12,23]. Transmission electron microscopy (TEM, Hitachi H-7650) images of the samples were also obtained.

2.3. Activity test

The catalytic activity test for hydriodic acid (7.4 mol/L, analytical reagent, Rizhao Lideshi Chemical Co., Ltd.) decomposition was performed in a quartz tubular reactor (outer diameter of 14 mm, inner diameter of 12 mm) under the following conditions: catalyst mass of 100 mg, reaction temperatures of 400 and 500 °C, and hydriodic acid flow rate of 1.0 mL/min under atmospheric pressure. The detailed activity evaluation of the catalysts was reported in a previous publication [23]. After the reaction, the catalyst was cooled to room temperature. TEM images were obtained to characterize the morphology of the used catalysts.

3. Results and discussion

3.1. Activity comparisons of the bimetallic and monometallic catalysts

Fig. 1 shows the catalytic performances of the AC-supported Pt, Ir, and Pt-Ir catalysts for HI decomposition at 400 °C (Fig. 1a) and 500 °C (Fig. 1b). The activities of the bimetallic Pt-Ir/C catalysts are dependent on their compositions. The addition of appropriate amounts of Ir can considerably modify the catalytic activity of the Pt/C catalysts. Among the different Pt-Ir bimetallic catalysts and monometallic Pt and Ir catalysts, the 2.5%Pt-2.5%Ir/C catalyst shows the highest activity under the same experimental conditions. With the increase in Ir content in the Pt-Ir bimetallic catalysts, the number of Pt atoms decreases and the number of Ir atoms increases on the exterior surface of the active metal particles. The monometallic 5%Ir/C also exhibits a lower activity than the monometallic 5%Pt/C. The 2.5%Pt-2.5%Ir/C catalyst also has much higher activity than the physical mixture Mix-2.5%Pt-2.5%Ir/C, which was prepared from the physical mixture of the monometallic 5%Pd/C and 5%Ir/C. Therefore, compared with the monometallic Pt or Ir catalysts, the relatively higher catalytic activity of the bimetallic Pt-Ir catalysts can be attributed to the interaction of the Pt and Ir metals.

Table 1
The average crystallite size calculated using Scherrer equation from XRD results.

Sample	2θ (°)	Index	Crystallite size (nm)
Used-5%Pt/C	39.960	1 1 1	18.7
Used-4%Pt-1%Ir/C	39.793	1 1 1	15.3
Used-3%Pt-2%Ir/C	39.846	1 1 1	13.8
Used-2.5%Pt-2.5%Ir/C	39.857	1 1 1	8.5
Used-2%Pt-3%Ir/C	40.026	1 1 1	6.7
Used-1%Pt-4%Ir/C	40.375	1 1 1	4.3

3.2. XRD patterns of fresh and used catalysts

The XRD patterns of the fresh Pt-Ir bimetallic catalysts are shown in Fig. 2. The broad diffraction peaks at approximately 25° in all of the XRD patterns show that the AC support has an amorphous structure. The two peaks of the (1 1 1) and (2 0 0) crystalline planes integrate into one broad peak, and the (2 2 0) and (3 1 1) diffraction peaks are absent. Thus, the Pt-Ir particles are highly dispersed on the carbon support. Both metallic Pt and Ir have the same face-centered cubic (FCC) crystalline structure. The total loading of Pt and Ir in each of the Pt-Ir catalysts is 5.0 wt.%. Therefore, no significant differences are found in the XRD patterns of all of the Pt-Ir catalysts.

Fig. 3 displays the XRD patterns of the used 5%Pt/C monometallic catalysts and Pt-Ir/C bimetallic catalysts. The typical Pt diffraction peaks at approximately 39.9° (1 1 1), 46.4° (2 0 0), 67.7° (2 2 0), and 81.5° (3 1 1) are found in the XRD patterns of the used 5%Pt/C. The four diffraction peaks of the corresponding crystalline planes can also be found in the XRD patterns of all of the Pt-Ir bimetallic catalysts. Thus, the used Pt-Ir/C bimetallic catalysts have the same FCC structure as the used Pt/C monometallic catalysts. However, the diffraction peaks in the used Pt catalysts are sharper and stronger than those in the used Pt-Ir catalysts. As the content of Ir increases, the diffraction peaks in the used Pt-Ir catalysts become weaker and broader. The average particle sizes were calculated from the (1 1 1) peaks using Scherrer equation (Table 1). After HI decomposition, the average particle sizes in the used 5%Pt/C, 3%Pt-2%Ir/C, 2.5%Pt-2.5%Ir/C, 2%Pt-3%Ir/C, and 1%Pt-4%Ir/C are 18.7, 13.8, 8.5, 6.7, and 4.3 nm, respectively. The results show that the increase in the Ir content of Pt-Ir catalysts improves their anti-sintering property and stability.

3.3. TEM images of fresh and used catalysts

Fig. 4 shows the TEM images of the 4%Pt-1%Ir/C, 3%Pt-2%Ir/C, 2.5%Pt-2.5%Ir/C, 2%Pt-3%Ir/C, and 1%Pt-4%Ir/C catalysts. The bimetallic Pt-Ir nanoparticles are uniformly dispersed on almost all of the catalysts with a narrow size distribution. Most of the par-

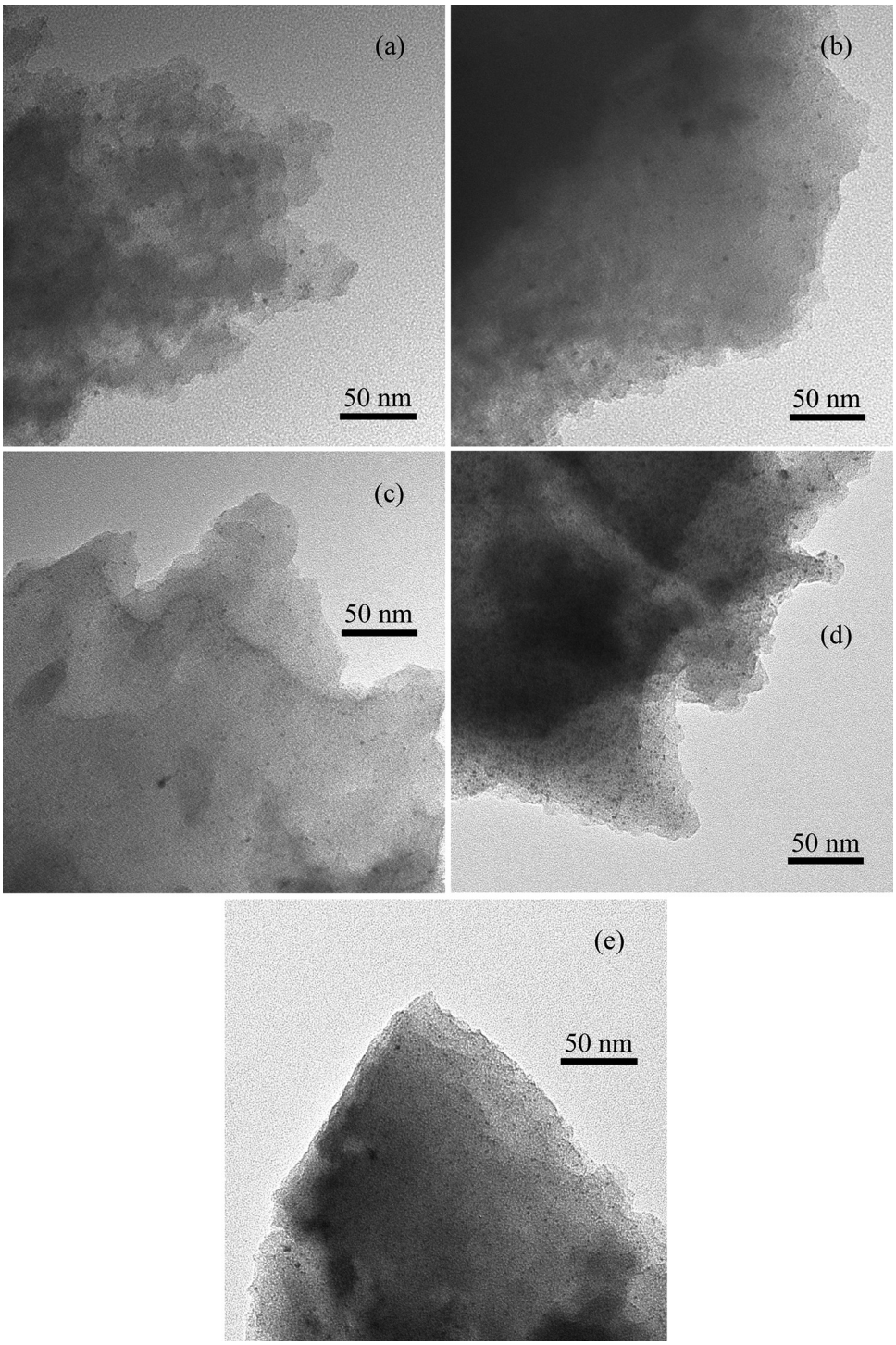

Fig. 4. TEM images of (a) 4%Pt-1%Ir/C, (b) 3%Pt-2%Ir/C, (c) 2.5%Pt-2.5%Ir/C, (d) 2%Pt-3%Ir/C, and (e) 1%Pt-4%Ir/C.

ticle diameters are in the range of 1–4 nm. Small differences are observed in the dispersion state or particle size among the various Pt-Ir catalysts, probably because all of the bimetallic Pt-Ir catalysts with the same total metal loadings are prepared using the same procedures.

The morphology and the particles size of the used monometallic Pt and bimetallic Pt-Ir catalysts are compared by TEM (Fig. 5). Obvious agglomeration of Pt nanoparticles can be found in the TEM image of the used 5%Pt/C, which indicates that the stability of the supported monometallic Pt catalysts is unsatisfactory for HI decomposition. This result is consistent with that of our previous study. The Pt-Ir bimetallic particles are better dispersed on the carbon support than the Pt monometallic particles. The TEM images also show that sintering of the nanoparticles occurs only in the used 4%Pt-1%Ir/C but not in the other used bimetallic Pt-Ir catalysts. The overall size of the particles also decreases with the increase in Ir content in the used Pt-Ir bimetallic catalysts. Fig. 6 shows the particle size distribution of the metal for the used monometallic Pt and bimetallic Pt-Ir catalysts. The mean particle size for the used 5%Pt/C, 4%Pt-1%Ir/C, 3%Pt-2%Ir/C, 2.5%Pt-2.5%Ir/C, 2%Pt-3%Ir/C, and

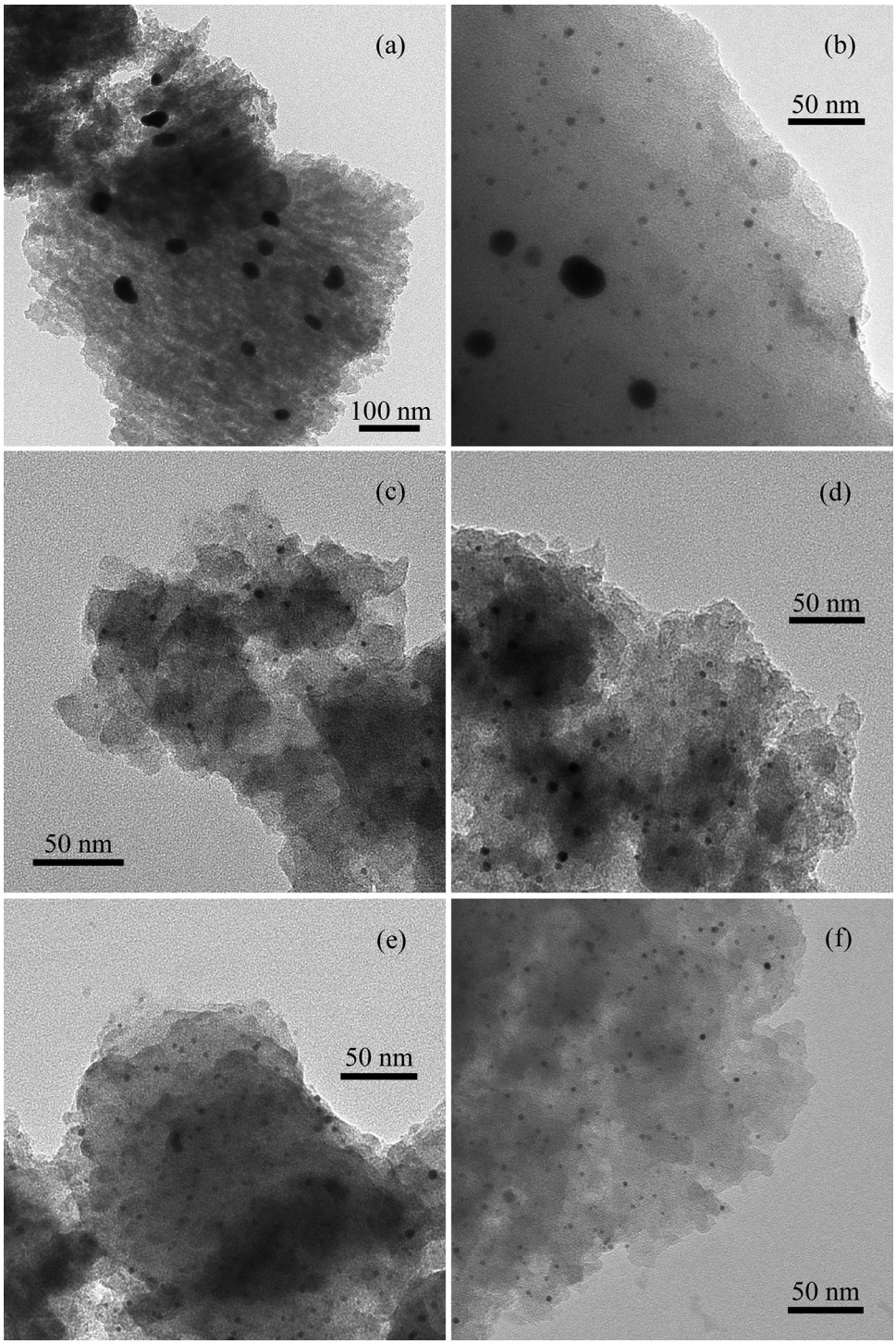

Fig. 5. TEM images of (a) used-5%Pt/C, (b) used-4%Pt-1%Ir/C, (c) used-3%Pt-2%Ir/C, (d) used-2.5%Pt-2.5%Ir/C, (e) used-2%Pt-3%Ir/C, and (f) used-1%Pt-4%Ir/C.

1%Pt-4%Ir/C are 25.6, 4.5, 4.3, 4.0, 3.8, and 3.1 nm, respectively. The TEM images and histograms of the particle size distributions show that introducing Ir into the supported Pt catalyst enables the small size and uniform distribution of supported metal nanoparticles, as well as promotes the stability of the catalysts. These results are consistent with the XRD results.

3.4. Long-term catalytic performance test

The bimetallic Pt-Ir catalysts with high stability exhibit long-term catalytic performance in HI decomposition. The long-term performance test was conducted at 500 °C for 70 h. Approximately 0.1 g of 2.5%Pt-2.5%Ir/C was used, and the flow rate of hydriodic acid was 0.5 mL/min. The results of the long-term catalytic performance of the Pt-Ir bimetallic catalysts are shown in Fig. 7. The conversions of HI fluctuate mildly at approximately 20%, and no obvious deactivation is found for the Pt-Ir bimetallic catalysts during the 70 h

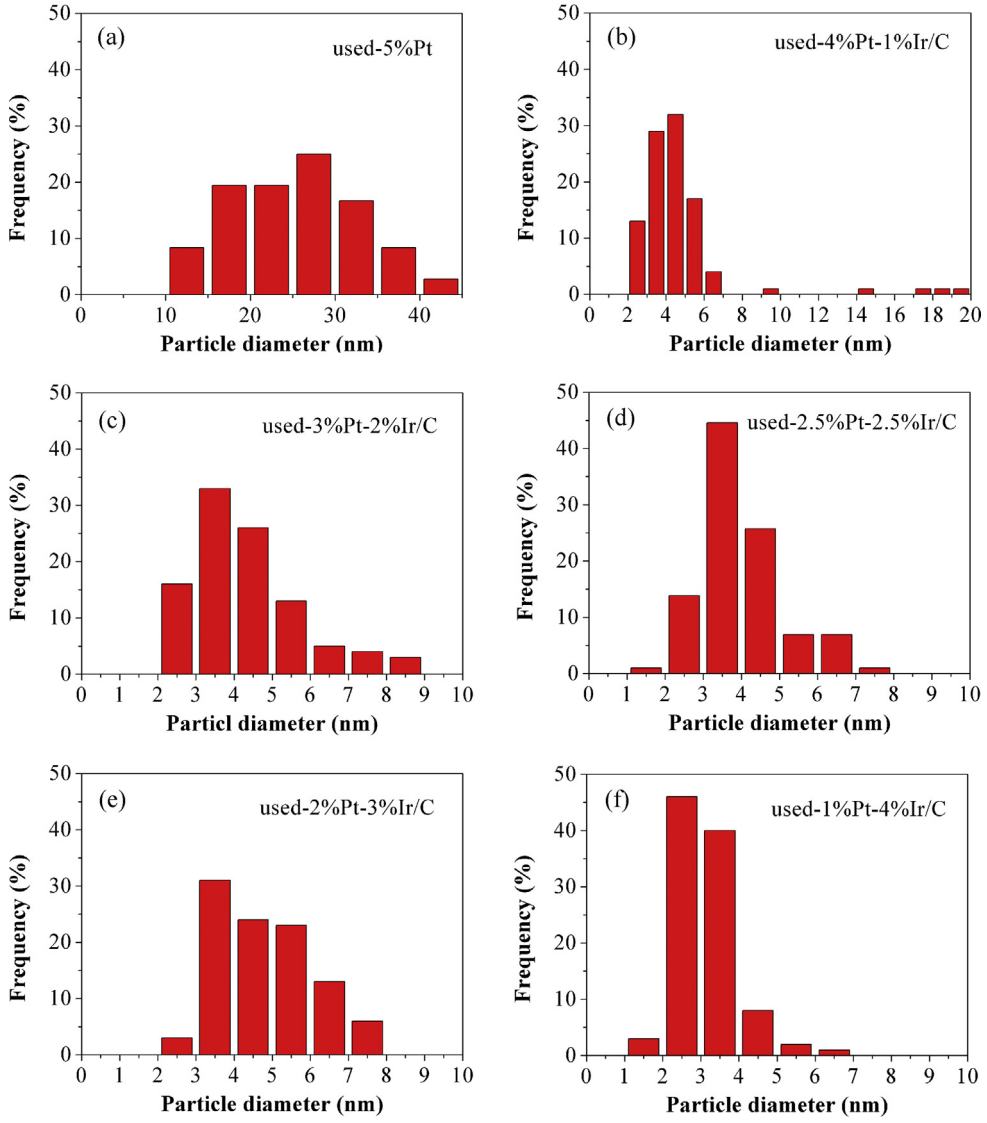

Fig. 6. Particle size distributions of (a) used-5%Pt/C, (b) used-4%Pt-1%Ir/C, (c) used-3%Pt-2%Ir/C, (d) used-2.5%Pt-2.5%Ir/C, (e) used-2%Pt-3%Ir/C, and (f) used-1%Pt-4%Ir/C.

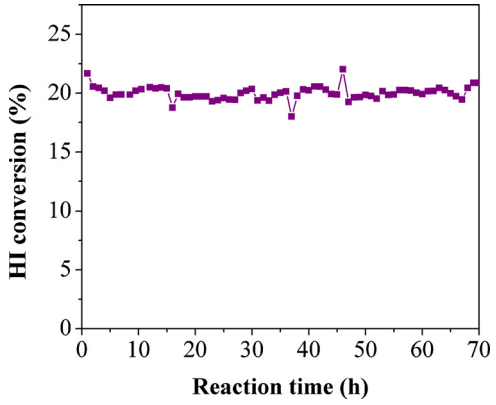

Fig. 7. HI conversion over the 2.5%Pt-2.5%Ir/C during the 70 h durability test.

durability test. Thus, the Pt-Ir bimetallic catalyst possesses good activity maintenance. Fig. 8 shows the TEM images of the 2.5%Pt-2.5%Ir after the 70 h durability test. The Pt-Ir bimetallic particles are homogeneous (ranging from 5 nm to 10 nm) and well-dispersed on the carbon support, which indicates that the Pt-Ir bimetallic catalysts possess excellent anti-sintering property compared with the monometallic Pt catalysts.

4. Conclusions

The AC-supported monometallic Pt and Ir catalysts, as well as the bimetallic catalysts with different Pt/Ir ratios, were prepared by impregnation–reduction method. According to the comparative characterizations of the fresh and used catalysts, the Pt-Ir bimetallic catalysts exhibit better stability than the monometallic Pt catalysts. Therefore, the interaction between Pt and Ir can enhance the stability of the Pt-Ir catalysts. The long-term catalytic performance tests reveal that the Pt-Ir bimetallic catalysts possess good activity maintenance. Given that the introduction of Ir into the supported Pt catalyst can not only decrease the content of the expensive metal Pt but can also improve the properties (such as the improved distribution of the supported metal nanoparticles and enhanced stability), the Pt-Ir bimetallic catalyst is a promising alternative to the traditional monometallic Pt catalyst for HI decomposition.

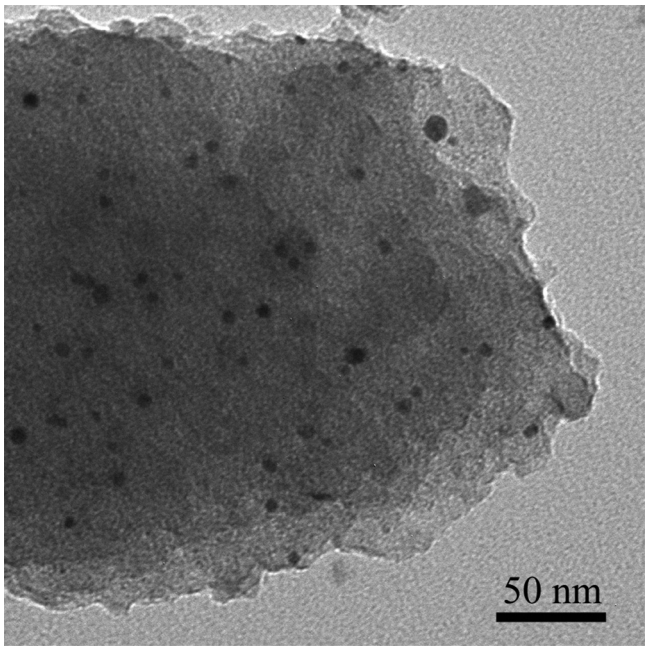

Fig. 8. TEM image of the 2.5%Pt-2.5%Ir after 70 h durability test.

Acknowledgments

This work was supported by the New Teacher Fund of Ministry of Education (200800031041), and Chinese National S&T Major Projects (2010zx06901).

References

[1] K. Onuki, S. Kubo, A. Terada, N. Sakaba, R. Hino, Energy Environ. Sci. 2 (2009) 491–497.
[2] X.L. Yan, R. Hino, Nuclear Hydrogen Production Handbook, Taylor & Francis Group, CRC Press, Boca Raton, 2011.
[3] P. Favuzza, C. Felici, L. Nardi, P. Tarquini, A. Tito, Appl. Catal. B-Environ. 105 (2011) 30–40.
[4] A.M. Banerjee, A.R. Shirole, M.R. Pai, A.K. Tripathi, S.R. Bharadwaj, D. Das, P.K. Sinha, Appl. Catal. B-Environ. 127 (2012) 36–46.
[5] P. Zhang, S.Z. Chen, L.J. Wang, J.M. Xu, Int. J. Hydrogen Energy 35 (2010) 2883–2887.
[6] X. Vitart, P. Carles, P. Anzieu, Prog. Nucl. Energy 50 (2008) 402–410.
[7] D.R. Okeefe, J.H. Norman, D.G. Williamson, Catal. Rev.-Sci. Eng. 22 (1980) 325–369.
[8] L.M. Petkovic, D.M. Ginosar, H.W. Rollins, K.C. Burch, C. Deiana, H.S. Silva, M.F. Sardella, D. Granados, Int. J. Hydrogen Energy 34 (2009) 4057–4064.
[9] L.J. Wang, D.C. Li, P. Zhang, S.Z. Chen, J.M. Xu, Int. J. Hydrogen Energy 37 (2012) 6415–6421.
[10] P. Favuzza, C. Felici, M. Lanchi, R. Liberatore, C.V. Mazzocchia, A. Spadoni, P. Tarquini, A.C. Tito, Int. J. Hydrogen Energy 34 (2009) 4049–4056.
[11] J.M. Kim, J.E. Park, Y.H. Kim, K.S. Kang, C.H. Kim, C.S. Park, K.K. Bae, Int. J. Hydrogen Energy 33 (2008) 4974–4980.
[12] L.J. Wang, S.K. Bai, Z.C. Wang, Y.L. Zhao, X. Yuan, P. Zhang, S.Z. Chen, J.M. Xu, X.H. Meng, Int. J. Hydrogen Energy 37 (2012) 10020–10027.
[13] S. Kubo, H. Nakajima, S. Kasahara, S. Higashi, T. Masaki, H. Abe, K. Onuki, Nucl. Eng. Des. 233 (2004) 347–354.
[14] P. Zhang, S.Z. Chen, L.J. Wang, T.Y. Yao, J.M. Xu, Int. J. Hydrogen Energy 35 (2010) 10166–10172.
[15] V. Dal Santo, A. Gallo, A. Naldoni, M. Guidotti, R. Psaro, Catal. Today 197 (2012) 190–205.
[16] W.T. Yu, M.D. Porosoff, J.G.G. Chen, Chem. Rev. 112 (2012) 5780–5817.
[17] N. Macleod, J.R. Fryer, D. Stirling, G. Webb, Catal. Today 46 (1998) 37–54.
[18] R.W. Rice, D.C. Keptner, Appl. Catal. A-Gen. 262 (2004) 233–239.
[19] O.B. Yang, S.I. Woo, R. Ryoo, J. Catal. 137 (1992) 357–367.
[20] O.B. Yang, S.I. Woo, I.C. Hwang, Catal. Lett. 19 (1993) 239–245.
[21] S.A. D'Ippolito, L.B. Gutierrez, C.L. Pieck, Appl. Catal. A-Gen. 445 (2012) 195–203.
[22] Z.C. Wang, L.J. Wang, S.Z. Chen, P. Zhang, J.M. Xu, J. Chen, Int. J. Hydrogen Energy 35 (2010) 8862–8867.
[23] L.J. Wang, Q. Han, D.C. Li, Z.C. Wang, J. Chen, S.Z. Chen, P. Zhang, B.J. Liu, M.F. Wen, J.M. Xu, Int. J. Hydrogen Energy 38 (2013) 109–116.